Chemical Science

EDGE ARTICLE

View Article Online
View Journal | View Issue

Cite this: *Chem. Sci.*, 2018, **9**, 5640

A bimetallic oxide $Fe_{1.89}Mo_{4.11}O_7$ electrocatalyst with highly efficient hydrogen evolution reaction activity in alkaline and acidic media†

Zhaomin Hao,[a] Shishuai Yang,[a] Jingyang Niu,[a] Zhiqiang Fang,[a] Liangliang Liu,[b] Qingsong Dong,*[a] Shuyan Song[c] and Yong Zhao*[b]

Received 14th April 2018
Accepted 26th May 2018

DOI: 10.1039/c8sc01710g

rsc.li/chemical-science

Transition-metal Mo-based materials have been considered to be among the most effective hydrogen evolution reaction (HER) electrocatalysts. Regulating the electronic structure of Mo atoms with guest metal atoms is considered as one of the important strategies to improve their HER activity. However, introduction of guest metal elements in the vicinity of Mo sites with atomic-level hybridization is difficult to realize, resulting in the failure of the modified electronic structure of Mo sites. Herein, an $Fe_{1.89}Mo_{4.11}O_7/MoO_2$ material is prepared through the thermal treatment of a ferrimolybdate precursor. It exhibits a Tafel slope of 79 mV dec^{-1} and an exchange current density of 0.069 mA cm^{-2} in 1 M KOH medium, as well as a Tafel slope of 47 mV dec^{-1} and an exchange current density of 0.072 mA cm^{-2} in 0.5 M H_2SO_4 medium. Compared to original Mo-based oxides, $Fe_{1.89}Mo_{4.11}O_7$ with the regulated Mo electronic structure shows a more suitable Mo–H bond strength for the fast kinetics of the HER process. Density functional theory (DFT) calculations also indicate that the Mo–H bond strength in $Fe_{1.89}Mo_{4.11}O_7$ is similar to the Pt–H bond strength, resulting in the high kinetic activity of Mo-based HER electrocatalysts in alkaline and acidic media.

Introduction

Electrolysis of water is an important component of hydrogen manufacturing technologies that can tackle the intense challenge of depletion of fossil fuels and increased environmental concerns.[1–3] The hydrogen evolution reaction (HER) is the essential reaction in water electrolysis, and requires an effective electrocatalyst to decrease the reaction energy barrier and increase the energy conversion efficiency.[4] Many research studies have already shown that Pt and its alloys are the best electrocatalysts due to their fast and stable reaction kinetics, but their high cost and scarcity limit their widespread application.[5] Great efforts have been devoted to the design and synthesis of alternative HER electrocatalysts based on cheap and earth-abundant metal elements, such as non-precious metal oxides (*e.g.* NiO and Mo–$W_{18}O_{49}$), carbides (*e.g.* WC and Mo_2C), phosphides (*e.g.* CoP, MoP and FeP), sulfides (*e.g.* Ni_3S_2 and MoS_2), *etc.*[6] Among all of these alternatives, transition-metal Mo-based materials are some of the most efficient HER electrocatalysts to date. In the family of Mo-based materials, molybdenum carbides, nitrides, sulfides and oxides are reported to be efficient and stable HER catalysts.[7] To achieve good HER activity of Mo-based catalysts, two types of strategies are often proposed: (1) improving the density of Mo active sites (D_{cas}), and (2) increasing the effective surface area (S_{eff}). For instance, our group prepared a MoCN nanocatalyst by using an *in situ* CO_2 emission strategy and the abundant amino group-based polydiaminopyridine precursors, which substantially improved the D_{cas} of Mo.[8] Chen *et al.* fabricated a $NiMoN_x$/C electrocatalyst by nitridation of NiMo bimetals with ammonia gas, demonstrating that the imprinting of NiMo nanopowders on high-surface-area carbon nanoparticles could largely improve the S_{eff}.[9]

Apart from the two strategies mentioned above, regulating the electronic structure (E_s) of Mo atoms is another important strategy to improve the HER activity of Mo-based catalysts. Introduction of guest non-metal or metal atoms can meet this demand. It potentially achieves a suitable metal–hydrogen bond strength between the Mo active site and hydrogen intermediates, resulting in the increased HER activity of Mo-based catalysts.[10] However, introduction of guest metal elements in the

[a]*Henan Key Laboratory of Polyoxometalate Chemistry, College of Chemistry and Chemical Engineering, Henan University, Kaifeng, 475004, Henan Province, P. R. China. E-mail: zmhao@henu.edu.cn*

[b]*Key Lab for Special Functional Materials of Ministry of Education, Collaborative Innovation Center of Nano Functional Materials and Applications, Henan University, Kaifeng, 475004, Henan Province, P. R. China. E-mail: zhaoyong@henu.edu.cn*

[c]*State Key Laboratory of Rare Earth Resource Utilization, Changchun Institute of Applied Chemistry, Chinese Academy of Sciences, Changchun 130022, P. R. China*

† Electronic supplementary information (ESI) available: Experimental details, TG, EDX, additional XPS results, SEM, TEM, related electrochemical curves, comparison of the HER performance with that of other HER electrocatalysts and related DFT details. See DOI: 10.1039/c8sc01710g

vicinity of Mo sites is difficult to realize to achieve the atomic-level hybridization of Mo and other metals.[7c] This is due to the fact that the starting precursors in the reported strategies are always based on the hybridization of Mo-based salt with other metal salts in the micro-sized state. Pyrolyzing such precursors can't produce a good dispersion of guest metal atoms in the Mo-based catalysts, resulting in the failure of the electronic structure of Mo active sites. Doping non-metal elements seems to be more controllable to modulate the electronic structure of Mo sites compared to those of metal atoms.[7b] However, non-metal atoms could potentially be removed from Mo sites under environmental conditions. For example, neither MoC nor MoN is stable enough in oxygen-containing environments or alkaline medium, and molybdenum oxides will cover the material surface.[9,10] Therefore, most of the materials still possess high HER overpotentials, thus impeding further improvement of their electrocatalytic activity.

In this work, an $Fe_{1.89}Mo_{4.11}O_7$ electrocatalyst was prepared by the thermal treatment of a ferrimolybdate precursor, an organic–inorganic compound which was synthesized by the self-assembly of Fe^{3+} and polymolybdate species. By using the ferrimolybdate as a precursor, the introduction of transition metal Fe atoms in the vicinity of Mo atoms at the atomic scale was realized in the $Fe_{1.89}Mo_{4.11}O_7$ based material. Compared to original Mo-based oxides, the modified electronic structure of Mo in $Fe_{1.89}Mo_{4.11}O_7$ induced the optimized metal–hydrogen bond strength. As a result, the kinetic activity was greatly improved with this type of Mo-based catalyst. Moreover, the HER activity of the as-prepared $Fe_{1.89}Mo_{4.11}O_7/MoO_2$ was much better than that of an Fe/MoO_2 electrocatalyst synthesized by pyrolyzing the hybrid of Fe^{3+} and a polymolybdate precursor. Theoretical calculations further confirmed that Fe-coordinated Mo sites did help to regulate the electronic structure of Mo active sites, which was beneficial for enhancing the HER activity of Mo-based catalysts.

Results and discussion

Fig. 1 shows the synthesis protocol for the preparation of different Mo-based materials. For obtaining the atom-scale blended Fe–Mo oxide (namely $Fe_{1.89}Mo_{4.11}O_7/MoO_2$), Fe-containing ferrimolybdate molecules ($[Fe(phen)_2(H_2O)]_2[PMo_{12}O_{40}]$)[11] (single crystals) were used as a precursor, which was treated *via* carburization and self-reduction reactions (producing low valence Mo),[12] followed by etching the unstable and inactive species from the pyrolyzed sample in 0.5 M H_2SO_4 solution to get the $Fe_{1.89}Mo_{4.11}O_7/MoO_2$ material. As a reference sample, a MoO_2 material without Fe was synthesized by using a similar polymolybdate (without Fe^{3+}, $[phen]_3[PMo_{12}O_{40}]$) as a precursor following the same pyrolysis protocol. Moreover, another reference sample, a non-atom-scale blended Fe–Mo oxide (named Fe/MoO_2), was synthesized by pyrolyzing the hybrid precursor of $FeCl_3$ and the polymolybdate ($[phen]_3[PMo_{12}O_{40}]$) to clarify the influence of Fe-coordination on the HER activity of Mo sites. Scheme S1† shows the chemical structure of polymolybdates and ferrimolybdates with Keggin anions and organic ligands (phenanthroline). Most of the organic components in the hybrid of Fe^{3+} and polymolybdates ultimately transformed into CO_2 when the pyrolysis temperature was above 600 °C. The transformation of ferrimolybdates required a higher temperature (about 800 °C) to achieve the same results (Fig. S1†). The differences of thermogravimetric temperatures in the hybrid of Fe^{3+} and polymolybdates, and ferrimolybdates for carbon element probably played an important role in carburization reactions.[7a] Using the hybrid of Fe^{3+} and polymolybdates as the precursor, Fe and Mo could not be in the atom-scale blended state and the self-reduction reaction was difficult to realize during the thermal treatment of $FeCl_3$ and polymolybdates.

The morphologies of the as-prepared Mo-based materials were checked by performing field-emission scanning electron microscopy (SEM) and transmission electron microscopy (TEM). Fig. 2a and b show the SEM images of the ferrimolybdate precursor and $Fe_{1.89}Mo_{4.11}O_7/MoO_2$ sample, indicating that they are basically massive structures. The SEM image in the inset of Fig. 2a demonstrates that the surface of the as-prepared ferrimolybdate precursor is roughly smooth, which is attributed to its single crystal properties. The SEM image of

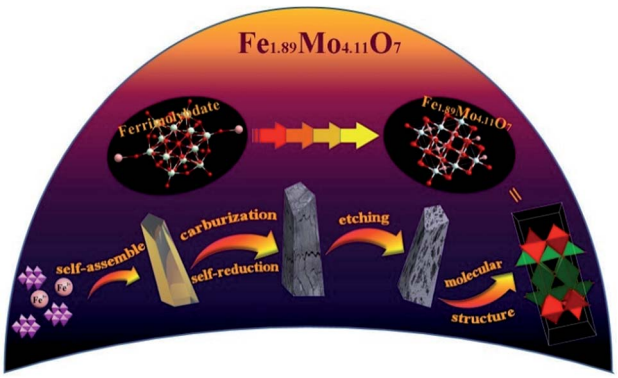

Fig. 1 Schematic illustration of the formation of $Fe_{1.89}Mo_{4.11}O_7$.

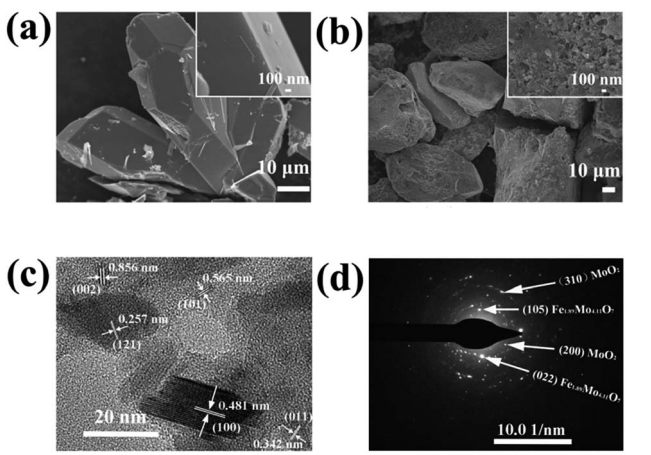

Fig. 2 SEM images of (a) the ferrimolybdate precursor and (b) the synthesized $Fe_{1.89}Mo_{4.11}O_7/MoO_2$ sample, and (c) HRTEM image and (d) SAED pattern of the $Fe_{1.89}Mo_{4.11}O_7/MoO_2$ sample.

$Fe_{1.89}Mo_{4.11}O_7/MoO_2$ shows that the surface of the Mo-based oxide is changed to a coarse and loose structure. Energy-dispersive X-ray (EDX) elemental mapping images based on an individual crystal particle confirm the coexistence and uniform distribution of Fe and Mo elements within the $Fe_{1.89}Mo_{4.11}O_7/MoO_2$ sample (Fig. S2†). From the high resolution TEM (HRTEM) image (Fig. 2c and S4†), the lattice spacing is about 0.481 nm, matching well with the (100) planes of the rhombohedral hexagonal phase of MoO_2. Moreover, the estimated lattice spacing of 0.257 nm can be indexed to the (121) planes of $Fe_{1.89}Mo_{4.11}O_7$. Importantly, the well-defined diffraction rings in the selected-area electron diffraction (SAED) pattern (Fig. 2d) confirm the polycrystalline nature of MoO_2 and $Fe_{1.89}Mo_{4.11}O_7$. These rings can be well indexed to the (310) and (200) planes of MoO_2 and the (105) and (022) crystal planes of $Fe_{1.89}Mo_{4.11}O_7$. All of the measurements confirmed that the $Fe_{1.89}Mo_{4.11}O_7$ material was successfully prepared using our synthesis protocol.

The crystalline structure of the as-synthesized products was checked by analyzing their powder X-ray diffraction (XRD) patterns. As shown in Fig. 3a, the XRD pattern of the $Fe_{1.89}Mo_{4.11}O_7/MoO_2$ material contains peaks of $Fe_{1.89}Mo_{4.11}O_7$ and MoO_2 (JSPCD no. 42-0317 and 73-1249). The characteristic diffraction peaks at 10.3, 15.7, 30.2 and 43.6 can be indexed to the (002), (101), (105) and (220) planes of $Fe_{1.89}Mo_{4.11}O_7$. The diffraction peaks at 18.4, 26.0, 31.8, 36.9, 53.5 and 63.5 can be indexed to the (100), (011), (−102), (−211), (−311) and (−123) planes of the MoO_2 crystal structure. In comparison, no diffraction peaks of $Fe_{1.89}Mo_{4.11}O_7$ are observed in the XRD patterns of MoO_2 and Fe/MoO_2 samples, and only MoO_2 peaks appear. This indicates that the ferrimolybdate is essential for the synthesis of the $Fe_{1.89}Mo_{4.11}O_7$ component in the $Fe_{1.89}Mo_{4.11}O_7/MoO_2$ material.

X-ray photoelectron spectroscopy (XPS) measurements were used to check the surface composition of our synthesized samples including that of MoO_2, MoO_2/Fe and $Fe_{1.89}Mo_{4.11}O_7/MoO_2$. The binding energies centred at 530.4 and 531.6 eV are ascribed to O_{1s},[12] while the binding energies of Fe_{2p} are located at 710.7 and 724 eV with a valence state of +3[13] (Fig. 3b and c). It is notable that the peak shape change for O_{1s} is due to the introduction of Fe element. Owing to pyrolyzing the organic–inorganic compound of ferrimolybdate in an Ar atmosphere, a C_{1s} peak centred at 284.3 eV can be detected. In the $Fe_{1.89}Mo_{4.11}O_7/MoO_2$ material, a small amount of carbon (5.3%) acted as a catalyst support owing to its good electrical conductivity (no molybdenum carbide is detected in the XRD pattern). To determine the composition of $Fe_{1.89}Mo_{4.11}O_7/MoO_2$, the peaks of Mo_{3d} were compared with those of MoO_2 and MoO_2/Fe. Compared to original Mo-based oxides, the introduction of Fe atoms can induce changes in electronegativity and modify the electronic structure of Mo. As shown in Fig. 3d, not only are the peak shapes very distinctive for $Fe_{1.89}Mo_{4.11}O_7/MoO_2$, but the position of some peaks is also shifted. The right peak in Mo_{3d} is shifted negatively by about 1.1 eV in comparison with those of MoO_2 and MoO_2/Fe samples. This indicates that the chemical environment of Mo is changed because of atom-scale blended Fe–Mo, and the electron density of Mo sites is enriched. This is proposed to be beneficial for the optimization of Mo–H bond strength in the HER process.

The electrocatalytic HER activity of the as-prepared Mo-based materials was evaluated in both alkaline and acidic aqueous solutions (pH 0.3 and pH 13.6). The HER activity of the $Fe_{1.89}Mo_{4.11}O_7/MoO_2$ catalyst was firstly optimized by pyrolyzing the precursors at different temperatures. As shown in Fig. S7,† the $Fe_{1.89}Mo_{4.11}O_7/MoO_2$ catalyst prepared at 1000 °C has the best performance, while the other samples show slightly inferior HER activity. Thus, all of the Mo-based catalysts prepared at 1000 °C are used for comparison of their HER activity. The $Fe_{1.89}Mo_{4.11}O_7/MoO_2$ catalyst shows an onset potential as low as ~70 mV in alkaline medium (pH 13.6) and ~40 mV in acidic medium (pH 0.3), which are estimated from the low current density region of the Tafel plot (Fig. S9 and S10†).[14] Fig. 4a and b show the electrocatalytic properties of HER catalysts under alkaline and acidic conditions, respectively. An overpotential of 197 mV is required for the $Fe_{1.89}Mo_{4.11}O_7/MoO_2$ catalyst to achieve a current density of 10 mA cm^{-2} in 1 M KOH. This value is much lower than those of the bare carbon paste (514 mV for 10 mA cm^{-2}), MoO_2 (431 mV for 10 mA cm^{-2}) and Fe/MoO_2 (322 mV for 10 mA cm^{-2}) samples (Fig. 4c and Table S1†). In addition, the electrocatalytic kinetics for the HER was analyzed using Tafel plots. As shown in Fig. S11,† the $Fe_{1.89}Mo_{4.11}O_7/MoO_2$ catalyst exhibits a small Tafel slope of 79 mV dec^{-1}, higher than 52 mV dec^{-1} for the 20% Pt/C catalyst. By extrapolating the Tafel plots, the value of exchange current density for the $Fe_{1.89}Mo_{4.11}O_7/MoO_2$ catalyst is calculated to be 0.069 mA cm^{-2} (Fig. S12†). In acidic electrolyte, it can be seen that the $Fe_{1.89}Mo_{4.11}O_7/MoO_2$ catalyst requires an overpotential of 125 mV to drive a current density of 10 mA cm^{-2} (Fig. 4c). The

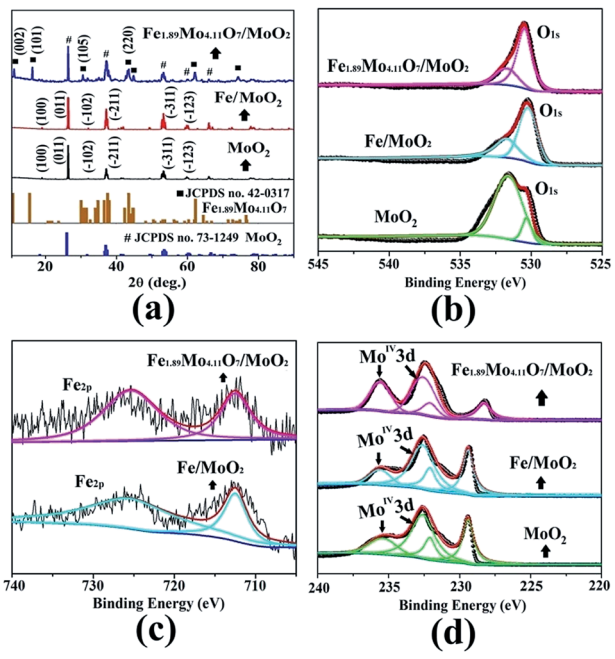

Fig. 3 The patterns of $Fe_{1.89}Mo_{4.11}O_7/MoO_2$, Fe/MoO_2 and MoO_2 (a) for XRD and XPS (b) O_{1s}, (c) Fe_{2p}, and (d) Mo_{3d}.

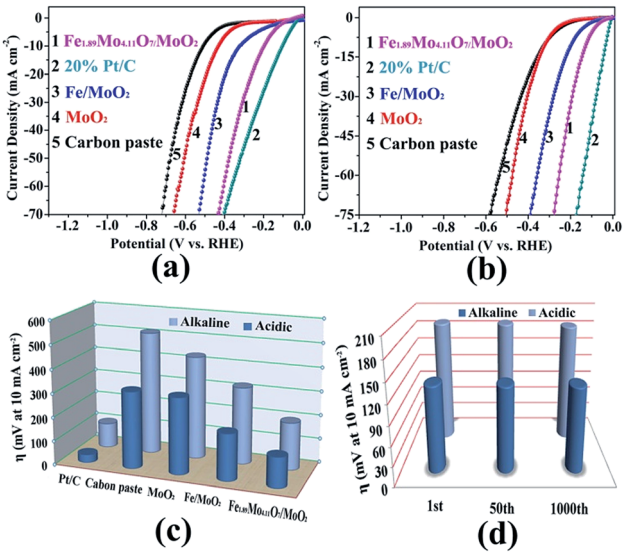

Fig. 4 HER performance of the Mo-based catalysts. (a) Polarization curves in 1 M KOH (pH 13.6), (b) polarization curves in 0.5 M H_2SO_4 (pH 0.3), (c) the HER activities expressed as potentials required to achieve a current density of 10 mA cm^{-2}, and (d) the changes at the current density of 10 mA cm^{-2} during continuous potential sweeps.

overpotential is much smaller than those of carbon paste (321 mV), MoO_2 (318 mV) and Fe/MoO_2 (194 mV) (Table S1†). As the sample composition has a significant effect on HER performance, XPS measurements were taken to check the fraction of each phase on the surface. In the $Fe_{1.89}Mo_{4.11}O_7/MoO_2$ sample, the atomic percentage of Fe is calculated to be 2.73%. Accordingly, the content of pure $Fe_{1.89}Mo_{4.11}O_7$ and MoO_2 is 15.8% and 78.9% in the mixture of $Fe_{1.89}Mo_{4.11}O_7/MoO_2$, respectively. When the $Fe_{1.89}Mo_{4.11}O_7/MoO_2$ sample was further etched by Ar sputtering at 1 Å s^{-1} for 100 s, there was no obvious change in the atomic percentage of Fe (2.65%, within a reasonable error range). This is due to the fact that Fe element is uniformly distributed in the $Fe_{1.89}Mo_{4.11}O_7/MoO_2$ product, which is deduced from the good distribution of Fe atoms at the atomic scale in the $[Fe(phen)_2(H_2O)]_2[PMo_{12}O_{40}]$ precursor. For the $Fe_{1.89}Mo_{4.11}O_7/MoO_2$ catalyst, a 15.8% content of $Fe_{1.89}Mo_{4.11}O_7$ results in a substantially decreased HER overpotential, leading to superior HER activity for $Fe_{1.89}Mo_{4.11}O_7$. The low HER overpotential at a current density of 10 mA cm^{-2} for the $Fe_{1.89}Mo_{4.11}O_7/MoO_2$ catalyst is also comparable to the values reported for most Mo-related HER catalysts in acidic aqueous media, such as MoS_2/RGO (140 mV for 10 mA cm^{-2}), MoO_3/MoS_2 (250 mV for 10 mA cm^{-2}), $MoSe_2$/Mo (166 mV for 10 mA cm^{-2}), *etc.*[15] (Table S2†). Similarly, the Tafel plots depicted in Fig. S12† also show a small Tafel slope of 47 mV dec^{-1} for the $Fe_{1.89}Mo_{4.11}O_7/MoO_2$ catalyst in 0.5 M H_2SO_4, along with an exchange current density of ~0.072 mA cm^{-2} (Fig. S14†).

To assess the durability of the $Fe_{1.89}Mo_{4.11}O_7/MoO_2$ electrocatalyst, linear potential sweeps were conducted at a scan rate of 20 mV s^{-1} in acidic and alkaline media. As shown in Fig. 4d and S15,† the polarization curve displays no shift during the first 50 sweeps at 10 mA cm^{-2} in both alkaline and acidic aqueous solutions. After continuous scanning for 1000 cycles, the polarization curves show only a little shift at a current density of 10 mA cm^{-2}, indicating that $Fe_{1.89}Mo_{4.11}O_7/MoO_2$ is stable over a wide pH range. The *i*–*t* measurements reveal that the $Fe_{1.89}Mo_{4.11}O_7/MoO_2$ electrocatalyst can maintain good catalytic activity in alkaline solution for at least 25 h (Fig. S16†). In order to clarify the stability of $Fe_{1.89}Mo_{4.11}O_7/MoO_2$ before and after hydrolysis, we checked its morphology by performing TEM measurements (Fig. S17†). No change of $Fe_{1.89}Mo_{4.11}O_7/MoO_2$ can be found. This demonstrates the good stability of the $Fe_{1.89}Mo_{4.11}O_7/MoO_2$ electrode for the HER in both alkaline and acidic environments.

To gain insight into the electrocatalytic activity of $Fe_{1.89}Mo_{4.11}O_7/MoO_2$, the HER curves are normalized by the amount of active sites and specific surface areas. According to the XPS results, the ratio of the Mo content on the surface of MoO_2, Fe/MoO_2 and $Fe_{1.89}Mo_{4.11}O_7/MoO_2$ is about 1 : 1 : 0.75. After normalizing the HER current densities based on Mo content, $Fe_{1.89}Mo_{4.11}O_7/MoO_2$ still shows better electrocatalytic activity than those of MoO_2 and Fe/MoO_2 materials (Fig. 5a). Based on the results of Brunauer–Emmett–Teller (BET) analysis, the specific surface areas of Fe/MoO_2 and $Fe_{1.89}Mo_{4.11}O_7/MoO_2$ are 22.8 m^2 g^{-1} and 45.5 m^2 g^{-1}, respectively (Fig. 5b). When the

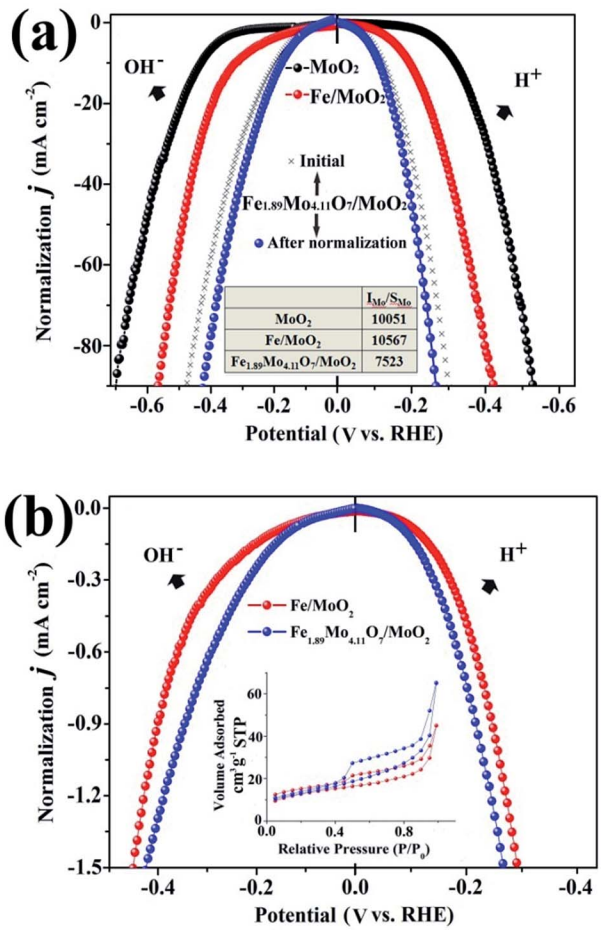

Fig. 5 The HER curves normalized by (a) active sites (based on Mo) and (b) specific surface areas.

HER curves are normalized by BET surface areas, the difference in the electrocatalytic activity between Fe/MoO_2 and $Fe_{1.89}Mo_{4.11}O_7/MoO_2$ is narrow but the absolute high-low tendency isn't changed (Fig. 5b). This indicates that the kinetic activity of Mo sites in $Fe_{1.89}Mo_{4.11}O_7$ is much higher than in MoO_2 and Fe/MoO_2 materials.

To further clarify the nature of the high HER activity of Mo sites in $Fe_{1.89}Mo_{4.11}O_7$, density functional theory (DFT) calculation using the Vienna *Ab initio* Simulation Package (VASP) was employed to understand the origin of the HER activity of the $Fe_{1.89}Mo_{4.11}O_7/MoO_2$ catalyst. It was already demonstrated that a good HER catalyst should have moderate metal–hydrogen bond strength.[16] Neither strong nor weak binding conditions of hydrogen intermediates would be beneficial for the overall HER reaction with a fast reaction rate, because the strong or weak binding conditions lead to either difficulty in removing the final product (H_2) or poor adsorption of the reactant (H^+). Herein, the metal–hydrogen (M–H) bond strength in $Fe_{1.89}Mo_{4.11}O_7$ is calculated to compare the Mo active sites with those in other representative Mo-based oxides. As shown in Fig. S18,† there is a distinct difference between the Fe–H and the Mo–H bond strength in $Fe_{1.89}Mo_{4.11}O_7$. The Mo–H bond strength (309 kJ mol^{-1}) in $Fe_{1.89}Mo_{4.11}O_7$ is closer to the Pt–H bond strength, while the Fe–H bond strength (916 kJ mol^{-1}) deviates from the Pt–H bond strength greatly, suggesting that Mo atoms serve as active sites in $Fe_{1.89}Mo_{4.11}O_7$. In addition, the metal–hydrogen bond strength of $Fe_{1.89}Mo_{4.11}O_7$ is also different from those of MoO_2 (24 kJ mol^{-1}), Mo_5O_{14} (206 kJ mol^{-1}) and Mo_8O_{23} (428 kJ mol^{-1}) (Fig. 6), indicating that the introduction of Fe in the vicinity of Mo sites indeed regulates the electronic structure of molybdenum active sites, resulting in a highly efficient Mo-based catalyst. As is well established, Pt is considered as one of the most excellent electrocatalysts for fast reaction kinetics. As shown in Fig. 6, the Mo–H bond strength in $Fe_{1.89}Mo_{4.11}O_7$ is closer to the Pt–H bond strength compared to other Mo-based oxides, suggesting that $Fe_{1.89}Mo_{4.11}O_7$ has more effective Mo active sites.

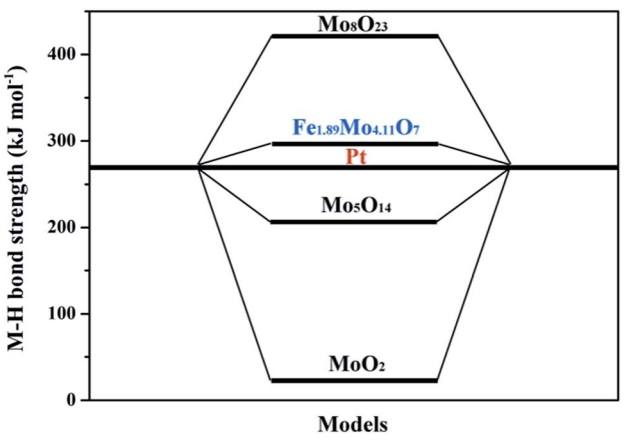

Fig. 6 The density functional theory (DFT) calculation of the metal–hydrogen (M–H) bond strength of the representative Mo-based oxides and Pt.

Conclusions and outlook

In summary, a novel binary $Fe_{1.89}Mo_{4.11}O_7$ electrocatalyst was prepared by the thermal treatment of a ferrimolybdate organic–inorganic hybrid. Benefiting from the modified electronic structure of Mo sites, the $Fe_{1.89}Mo_{4.11}O_7/MoO_2$ material showed highly efficient HER activity in both alkaline and acidic media. Further work on improving the purity of $Fe_{1.89}Mo_{4.11}O_7$ will substantially improve the HER activity from the viewpoint of active site enrichment. This work has profound experimental and theoretical significance in the field of polyoxometals and their applications, and it will inspire rational creation of new binary Mo-related oxides for advanced electrocatalytic hydrogen production.

Conflicts of interest

The authors declare no conflicts of interest.

Acknowledgements

The authors are grateful to the financial support from the National Natural Science Foundation of China (No. 21401203, 21702045, U1604122, 21773055 and 51702086), the Education Department of Henan Province (Grant 15A150035), Program for Science & Technology Innovation Talents in Universities of Henan Province (18HASTIT004), and the "1000 Youth Talents Plan" of China.

Notes and references

1 (*a*) A. J. Bard and M. A. Fox, *Acc. Chem. Res.*, 1995, **28**, 141–145; (*b*) J. Chow, R. J. Kopp and P. R. Portney, *Science*, 2003, **302**, 1528–1531.

2 (*a*) H. Zhong, J. Wang, F. Meng and X. Zhang, *Angew. Chem., Int. Ed.*, 2016, **55**, 10091–10095; (*b*) N. S. Lewis and D. G. Nocera, *Proc. Natl. Acad. Sci. U. S. A.*, 2006, **103**, 15729–15735; (*c*) J. Sun, H. Yin, P. Liu, Y. Wang, X. Yao, Z. Tang and H. Zhao, *Chem. Sci.*, 2016, **7**, 5640–5646; (*d*) S. Zhao, Y. Wang, J. Dong, C.-T. He, H. Yin, P. An, K. Zhao, X. Zhang, C. Gao, L. Zhang, J. Lv, J. Wang, J. Zhang, A. M. Khattak, N. A. Khan, Z. Wei, J. Zhang, S. Liu, H. Zhao and Z. Tang, *Nat. Energy*, 2016, **1**, 16184–16194.

3 (*a*) Z. Lu, M. Sun, T. Xu, Y. Li, W. Xu, Z. Chang, Y. Ding, X. Sun and L. Jiang, *Adv. Mater.*, 2015, **27**, 2361–2366; (*b*) R. C. Dustin, D. M. Aditya, M. G. Alejandro, M. Ulises, S. Andriy and J. Zhang, *Nat. Commun.*, 2016, **7**, 11857–11867; (*c*) Y. Shi, J. Wang, C. Wang, T. T. Zhai, W. J. Bao, J. J. Xu and X. H. Xia, *J. Am. Chem. Soc.*, 2015, **137**, 7365–7370; (*d*) H. Yin and Z. Tang, *Chem. Soc. Rev.*, 2016, **45**, 4873–4891.

4 (*a*) M. G. Walter, E. L. Warren, J. R. McKone, S. W. Boettcher, Q. Mi, E. A. Santori and N. S. Lewis, *Chem. Rev.*, 2010, **110**, 6446–6473; (*b*) H. Yin, S. Zhao, K. Zhao, A. Muqsit, H. Tang, L. Chang, H. Zhao, Y. Gao and Z. Tang, *Nat. Commun.*, 2015, **6**, 6430–6438.

5 S. Zhang, Y. Z. Hao, D. Su, V. V. T. Doan-Nguyen, Y. T. Wu, J. Li, S. Sun and C. B. Murray, *J. Am. Chem. Soc.*, 2014, **136**, 15921–15924.

6 (*a*) Y. Xu, M. Gao, Y. Zheng, J. Jiang and S. Yu, *Angew. Chem., Int. Ed.*, 2013, **52**, 8546–8550; (*b*) J. Yang, D. Voiry, S. J. Ahn, D. Kang, A. Y. Kim, M. Chhowalla and H. S. Shin, *Angew. Chem., Int. Ed.*, 2013, **52**, 13751–13754; (*c*) Z. Lu, W. Zhu, X. Yu, H. Zhang, Y. Li, X. Sun, X. Wang, H. Wang, J. Wang, J. Luo, X. Lei and L. Jiang, *Adv. Mater.*, 2014, **26**, 2683–2687; (*d*) C. G. Morales-Guio and X. Hu, *Acc. Chem. Res.*, 2014, **47**, 2671–2681; (*e*) D. Kong, H. Wang, Z. Lu and Y. Cui, *J. Am. Chem. Soc.*, 2014, **136**, 4897–4900; (*f*) L. Liao, S. Wang, J. Xiao, X. Bian, Y. Zhang, M. D. Scanlon, X. Hu, Y. Tang, B. Liu and H. H. Girault, *Energy Environ. Sci.*, 2014, **7**, 387–392; (*g*) Q. Liu, J. Tian, A. M. Asiri and X. Sun, *Angew. Chem., Int. Ed.*, 2014, **53**, 6828–6832; (*h*) P. Jiang, Q. Liu, Y. Liang, J. Tian, A. M. Asiri and X. Sun, *Angew. Chem., Int. Ed.*, 2014, **53**, 12855–12859; (*i*) E. J. Popczun, C. G. Read, C. W. Roske, N. S. Lewis and R. E. Schaak, *Angew. Chem., Int. Ed.*, 2014, **53**, 5531–5534; (*j*) P. Xiao, X. Ge, H. Wang, Z. Liu, A. Fisher and X. Wang, *Adv. Funct. Mater.*, 2015, **25**, 1520–1526; (*k*) H. Tang, J. Wang, H. Yin, H. Zhao, D. Wang and Z. Tang, *Adv. Mater.*, 2015, **27**, 1117–1123; (*l*) L. Han, S. Dong and E. Wang, *Adv. Mater.*, 2016, **28**, 9266–9291; (*m*) C. L. Bentley, M. Kang, F. M. Maddar, F. Li, M. Walker, J. Zhang and P. R. Unwin, *Chem. Sci.*, 2017, **8**, 6583–6593.

7 (*a*) H. B. Wu, B. Y. Xia, L. Yu, X.-Y. Yu and X. W. Lou, *Nat. Commun.*, 2015, **6**, 6512–6519; (*b*) W.-F. Chen, C.-H. Wang, K. Sasaki, N. Marinkovic, W. Xu, J. T. Muckerman, Y. Zhu and R. R. Adzic, *Energy Environ. Sci.*, 2013, **6**, 943–951; (*c*) X. Xu, F. Nosheen and X. Wang, *Chem. Mater.*, 2016, **28**, 6313–6320; (*d*) X. Xie, L. Lin, R. Liu, Y. Jiang, Q. Zhu and A. Xu, *J. Mater. Chem. A*, 2015, **3**, 8055–8061; (*e*) X. Xie, R. Yu, N. Xue, A. B. Yousaf, H. Du, K. Liang, N. Jiang and A. Xu, *J. Mater. Chem. A*, 2016, **4**, 1647–1652; (*f*) L. Yang, W. Zhou, D. Hou, K. Zhou, G. Li, Z. Tang, L. Li and S. Chen, *Nanoscale*, 2015, **7**, 5203–5208; (*g*) Y. Jin and P. K. Shen, *J. Mater. Chem. A*, 2015, **3**, 20080–20085; (*h*) Y. Jin, H. Wang, J. Li, X. Yue, Y. Han, P. K. Shen and Y. Cui, *Adv. Mater.*, 2016, **28**, 3785–3790; (*i*) L. Wu, X. Wang, Y. Sun, Y. Liu and J. Li, *Nanoscale*, 2015, **7**, 7040–7044; (*j*) J.-S. Li, Y. Wang, C.-H. Liu, S.-L. Li, Y.-G. Wang, L.-Z. Dong, Z.-H. Dai, Y.-F. Li and Y.-Q. Lan, *Nat. Commun.*, 2016, **7**, 11204–11211.

8 Y. Zhao, K. Kamiya, K. Hashimoto and S. Nakanishi, *J. Am. Chem. Soc.*, 2015, **137**, 110–113.

9 W. F. Chen, K. Sasaki, C. Ma, A. I. Frenkel, N. Marinkovic, J. T. Muckerman, Y. M. Zhu and R. R. Adzic, *Angew. Chem., Int. Ed.*, 2012, **51**, 6131–6135.

10 M.-R. Gao, M. K. Y. Chan and Y. Sun, *Nat. Commun.*, 2015, **6**, 7493–7501.

11 (*a*) J. Q. Sha, J. Peng, H. S. Liu, J. Chen, A. X. Tian, B. X. Dong and P. P. Zhang, *J. Coord. Chem.*, 2008, **61**, 1221–1233; (*b*) Q. Zhang and C. Tian, *Chem. Bull.*, 2011, **74**, 942–946.

12 (*a*) J. Haber, T. Machej, L. Ungier and J. Ziolkowski, *J. Solid State Chem.*, 1978, **25**, 207–218; (*b*) T. A. Patterson, J. C. Carver, D. E. Leyden and D. M. Hercules, *J. Phys. Chem.*, 1976, **80**, 1700–1708.

13 (*a*) H. J. Mathieu and D. Landolt, *Corros. Sci.*, 1986, **26**, 547–559; (*b*) B. J. Tan, K. J. Klabunde and P. M. A. Sherwood, *Chem. Mater.*, 1990, **2**, 186–191.

14 W. F. Chen, K. Sasaki, C. Ma, A. I. Frenkel, N. Marinkovic, J. T. Muckerman, Y. Zhu and R. R. Adzic, *Angew. Chem., Int. Ed.*, 2012, **51**, 6131–6135.

15 (*a*) J. Kibsgaard, Z. B. Chen, B. N. Reinecke and T. F. Jaramillo, *Nat. Mater.*, 2012, **11**, 963–969; (*b*) M.-R. Gao, J.-X. Liang, Y.-R. Xu, J. Jiang, Q. Gao, J. Li and S.-H. Yu, *Nat. Commun.*, 2015, **6**, 5982–5989; (*c*) D. Voiry, H. Yamaguchi, J. Li, R. Silva, D. C. B. Alves, T. Fujita, M. Chen, T. Asefa, V. B. Shenoy and G. Eda, *Nat. Mater.*, 2013, **12**, 850–855; (*d*) Z. Chen, D. Cummins, B. N. Reinecke, E. Clark, M. K. Sunkara and T. F. Jaramillo, *Nano Lett.*, 2011, **11**, 4168–4175; (*e*) Y. Li, H. Wang, L. Xie, Y. Liang, G. Hong and H. Dai, *J. Am. Chem. Soc.*, 2011, **133**, 7296–7299; (*f*) H. Lin, Z. Shi, S. He, X. Yu, S. Wang, Q. Gao and Y. Tang, *Chem. Sci.*, 2016, **7**, 3399–3405; (*g*) Y. Qu, H. Medina, S. W. Wang, Y. C. Wang, C. W. Chen, T. Y. Chen, A. Manikandan, K. Wang, Y. C. Shi, J. W. Chang, H. C. Kuo, C. Y. Lee, S. Y. Lu, G. Shen, Z. M. Wang and Y. L. Chueh, *Adv. Mater.*, 2016, **28**, 9831–9838.

16 (*a*) B. E. Conway and G. Jerkiewicz, *Electrochim. Acta*, 2000, **45**, 4075–4083; (*b*) F. Calle-Vallejo, M. T. M. Kopera and A. S. Bandarenka, *Chem. Soc. Rev.*, 2013, **42**, 5210–5230.